

Short Communication

Cold rolled 304 stainless steel and its interaction with liquid Sn

Chuang-dong Zhang, Yan Zhao, Jian-jun Guan, Rong-hua Li, Feng Liu, Ping Liang*

School of Mechanical Engineering, Liaoning Shihua University, Fushun 113001, Liaoning, China

*E-mail: zhaoyan-a@163.com

Received: 6 May 2019 / Accepted: 15 July 2019 / Published: 5 August 2019

The effect of strain-induced α' -martensite transformation and subsequent solution treatment on the interaction between stainless steel and liquid metal Sn was investigated. Liquid metal corrosion and electrochemical corrosion behavior was evaluated. A cold rolling (CR) treatment was performed to induce different amounts of α' -martensite. The reduction ratio of 36%, 55%, and 78% was used, and solution treatment (ST) was carried out. The phase structure of the stainless steels was examined by XRD, and the morphology and composition of the compound were formed by SEM and EDX. The results show that the cold rolling deformation leads to a large amount of α' -martensite transformation, and the solution treatment causes some martensite return to austenite. The deformed stainless steel interacts with liquid Sn, forming a (Fe,Cr)Sn₂ phase compound layer. The amount of deformation increases, the fine needle-like compound gradually increases, while the compound of the lath-like morphology gradually decreases. After the solution treatment, the fine needle-like compound returns to the lath-like morphology. The cold rolling treatment induces the α' -martensitic transformation, resulting in a significant change in the growth the Fe-Sn compound. At the low deformations of 36% and 55%, the cold rolling is found to decrease the pitting potential, and deteriorates the electrochemical corrosion behavior of stainless steel. At the deformation of 78%, the pitting corrosion resistance is increased, and the compound thickness expresses a small change.

Keywords: Cold rolling, Austenitic stainless steel, Strain induced martensite, Electrochemical corrosion, Liquid metal corrosion

1. INTRODUCTION

Austenitic stainless steel has excellent corrosion resistance, oxidation resistance and mechanical processing property, so it is widely used in nuclear power plants, petrochemicals, aerospace and other industrial fields [1, 2]. The strength and plasticity of stainless steel can be varied depending on the processing conditions. In AISI 304 stainless steel, the strength of the material can be

increased by cold rolling due to its strain hardening [3]. However, various problems are introduced by the cold rolling deformation of metal material [4-6]. First, under the action of external stress, low temperature plastic deformation leads to dislocation slip and dislocation proliferation. Furthermore, cold rolling deformation causes material to elongate, and holes or cracks appear at the interface. Finally, austenitic stainless steel is susceptible to martensite transformation after cold working deformation. Austenitic microstructure which is without strain and carbide is typically produced by heating treatment above 1000 °C and then rapidly quenching to retain carbon in solution [7].

The influence of cold working deformation on the corrosion resistance of alloy steel has been attention to many researchers. Maric et al investigated the influence of cold working on the microstructure of 316L stainless steel in molten salt corrosion [8], and the results indicated the beneficial effect of cold working on corrosion resistance and mechanical property. The corrosion resistance of carbon steels is decreased as the increasing cold rolling amount, but for austenitic stainless steels, the relation between cold rolling and corrosion resistance is not clear [9]. Rodrigues studied the effect of low old working stain on microstructure, texture, phase transformation and mechanical property of 2304 lean duplex stainless steel [10]. Pitting corrosion behavior of stainless steel from a combination of electrochemical and metallurgical factors, has already been extensive attention [11-13]. The presence of martensite phase induced by cold rolling makes corrosion behavior of stainless steels relatively complex. Therefore, the pitting corrosion of stainless steel induced by strain need to be in depth studied.

During the processing, the stainless steel may be in contact with low melting point metals [14, 15], which are potentially present in engineering test fluids and marking materials such as paint, chalk, ink. The brittle failure for components can appear because of the long term service. Compounds formed by the interaction between metallic materials and liquid metals are the direct cause for equipment failure [16]. In the preliminary work of the research group, the interaction mechanism between stainless steel and low melting point metal Sn was studied [17-18], but the interaction between cold rolled stainless steel and liquid Sn was not studied in depth.

In this paper, the effect of strain-induced α' -martensite transformation and subsequent solution treatment on the interaction between stainless steel and liquid metal Sn was investigated. Cold rolling treatment was performed to induce different amounts of α' -martensite, and a reduction ratio of 36%, 55%, and 78% was used. The phase structure of the cold rolling stainless steel was examined, and the morphology and composition of the compound were detected. The relationship between pitting potential and growth compound thickness of strain-induced martensitic transformation stainless steel was discussed, and the failure mechanism of liquid metal corrosion and electrochemical corrosion of cold deformed stainless steel was revealed.

2. EXPERIMENTAL

The material used in the experiment was 304 austenitic stainless steel, and its main chemical composition (wt%) was: C 0.025, Cr 17.959, Ni 9.208, Mn 1.062, Si 0.635, Mo 0.091, S 0.005, P 0.019, and Fe. The samples were processed into 75 mm × 15 mm × 1.5 mm plate shape. The samples

were mechanically ground to 1200# emery paper, and were dried after deionized water washing. The samples were rolled in a laboratory mill to a thickness reduction of 36%, 55% and 78%. All rolled samples were solution treated in an inert gas oven at 1100 °C for 40 minutes and then water quenched.

The prepared samples were allowed to interact with molten Sn having a purity of 99.99% at 250 °C for 240 min. Surface attached Sn was dissolved by a solution including 90 vol.% ethanol, 10 vol.% nitric acid to observe the compound surface morphology. The samples were etched with a solution containing 93 vol.% ethanol, 5 vol.% nitric acid, and 2 vol.% hydrochloric acid to observe the cross section morphology. Scanning electron microscope (SEM, JSM5600-LV) was used in the test to observe the compound morphology. The rolled and annealed samples were tested for phase identification by X-ray diffraction (XRD-6000). The thickness of Fe-Sn intermetallics was measured by an imaging processing software (Image pro-Plus).

The electrochemical corrosion behavior of rolled and annealed stainless steel was detected by a CS350 electrochemical workstation. The sample was tested in 3.5% NaCl solution using a three-electrode system. The saturated calomel electrode (SCE) was the reference electrode, the platinum electrode was the auxiliary electrode, and the sample was the working electrode. The effective area was 0.942 cm². Potentiodynamic polarization was scanned from -0.7 to 1.0 V (SCE) at a scan rate of 1 mV/s.

3. RESULTS and DISCUSSION

3.1 Strain-induced martensite transformation

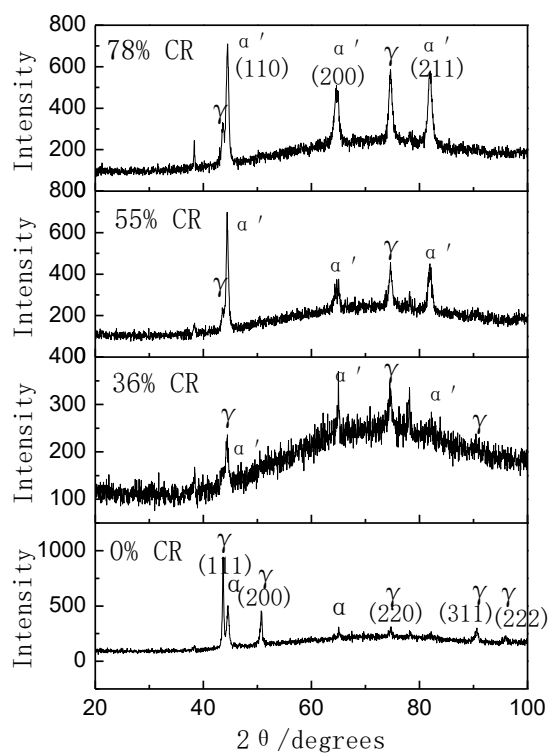


Figure 1. XRD pattern of 304 stainless steel under rolling deformation of 0%, 36%, 55% and 78%

Figure 1 shows the XRD pattern of AISI 304 stainless steel samples at 0%, 36%, 55%, and 78% rolling deformation. It can be seen from the experimental results that the rolling treatment leads to the development of the α' -martensitic peak. The intensity of the (110) (200) and (211) diffraction peaks gradually increases with the increasing the rolling reduction ratio. Observing the evolution of the austenite γ -phase diffraction peak, the intensity of the (111) crystal plane diffraction peak decreases, while the intensity of the (220) crystal plane diffraction peak increases, and the (311) and (222) diffraction peaks disappear after cold rolling deformation.

Figure 2 shows the microscopic topography of Fe-Sn intermetallics after the interaction between 304 stainless steel with different deformation and liquid Sn. It can be seen from Fig. 2 (a) that the stainless steel with a deformation of 0% reacts with Sn to form a sheet-like or lath-like compound at outer layer, and the inner layer forms fine granular compound. When the deformation is 36%, the outer lath-like compound is reduced, as shown in Fig. 2 (b). In Fig. 2 (c), the surface strip-shaped Fe-Sn compound is scattered, and the inner layer compound is finely needled, for stainless steel with a deformation amount of 55%. For the cold rolling of 78% sample, the compound, with a shape variable, has a thin rod-like morphology, and the slab-like morphology is few, as shown in Fig. 2 (d).

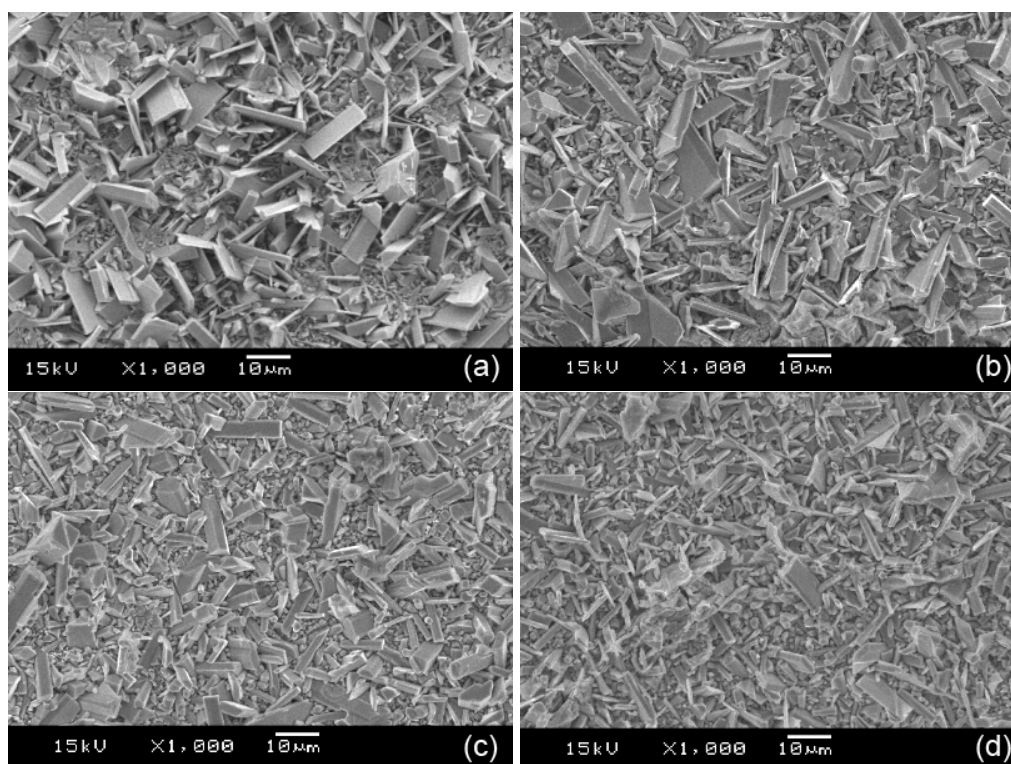


Figure 2. Surface morphology of Fe-Sn compound after the interaction between cold rolled 304 stainless steel and liquid Sn, (a) deformation amount of 0%, (b) deformation amount of 36%, (c) deformation amount of 55%, (d) deformation amount of 78%

Figure 3 shows the cross-sectional morphology of the compound formed by the interaction of different deformation of stainless steel with Sn. It can be seen that an intermetallics layer is grown between the stainless steel and Sn. The slab-like or fine-rod compound grows in the direction of Sn, and the dense compound grows near the layer of stainless steel. When the rolling deformation

increases from 0% (Fig. 3a) to 36% and 55% (Fig. 3b-c), the thickness of the compound layer gradually increases. But the Fe-Sn intermetallics thickness does not increase much for the stainless steel with a deformation amount of 78%, as shown in Fig. 3 (d).

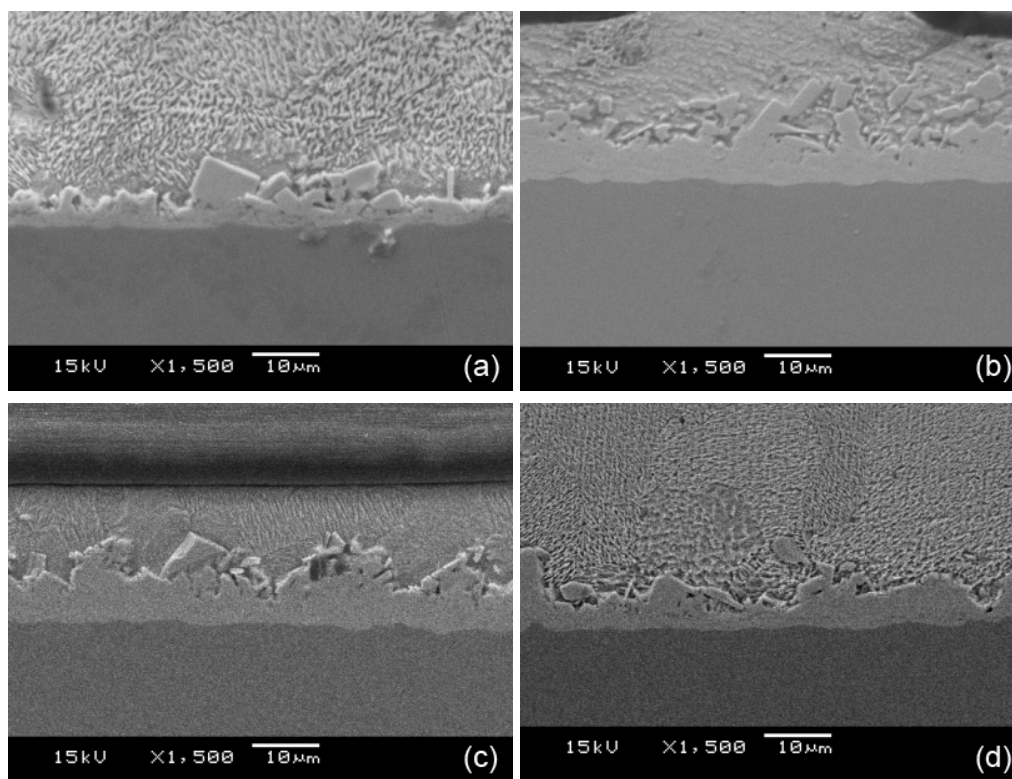


Figure 3. Cross section morphology of Fe-Sn compound after the interaction between cold rolled 304 stainless steel and liquid Sn, (a) deformation amount of 0%, (b) deformation amount of 36%, (c) deformation amount of 55%, (d) deformation amount of 78%

The phase structure of the compound formed by the interaction between stainless steel and Sn was detected, and the experimental results are shown in Fig. 4. For the stainless steel with the deformation of 0% and 55%, the FeSn_2 diffraction is detected. The EDX analysis shows that the compound contains 26.37 wt.% Fe, 3.98 at.% Cr, 69.95 at.% Sn. The Cr atom replaces the Fe atom, so the compound is a $(\text{Fe,Cr})\text{Sn}_2$ phase. Comparing the deformation variables between 0% and 55%, XRD results reveal that there is no γ diffraction peak in 55% deformation sample. It is related that the intermetallics thickness growth for the deformation of 55% (Fig. 3), and the X-ray could not be scanned to the stainless steel substrate.

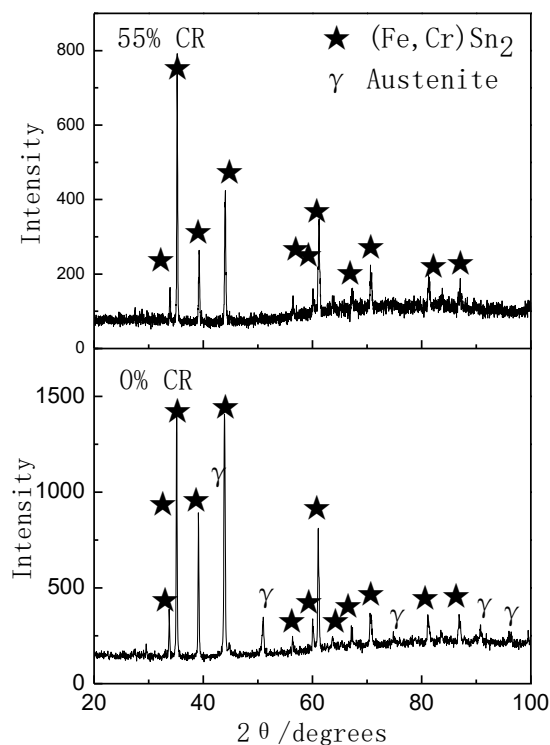


Figure 4. XRD patterns of the intermetallics on stainless steel surface with the deformation of 0% and 55%

3.2 Recrystallization behavior

The effect of solution treatment on the phase structure of the deformed stainless steel is shown in Fig. 5. Fig. 5(a) shows the XRD pattern of the stainless steel with 78% rolled deformation, and Fig. 5(b) shows the XRD pattern of the sample after solution treatment. The intensity of the α' -martensitic diffraction peaks of the (110) and (200) crystal faces is significantly reduced after solution treatment. The diffraction peak of (211) α' -martensite has disappeared. The diffraction peak of the γ austenite phase is enhanced.

The surface morphology of the compound formed on 78% cold rolled stainless steel and solution treatment stainless steel is shown in Fig. 6. The relatively small size intermetallics are observed on the cold rolled stainless steel, as shown in Fig. 6(a). The deformed stainless steel undergoes solution treatment, and the growth of the lath-like compound increases, displayed in Fig. 6(b).

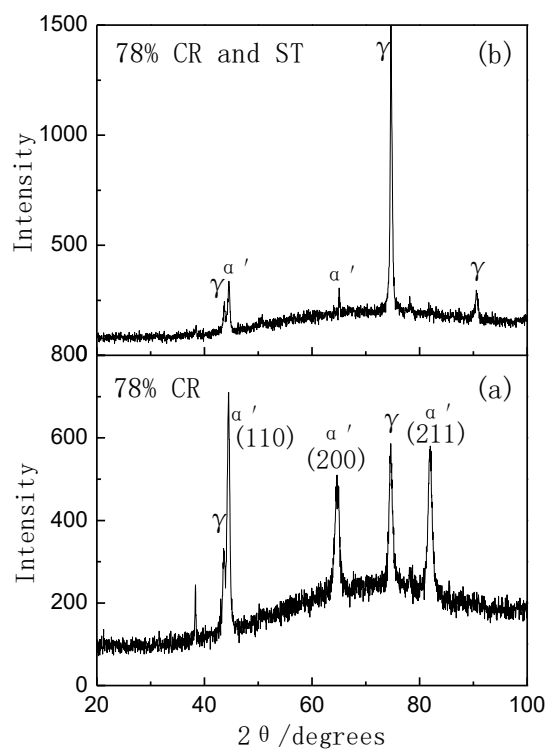


Figure 5. XRD patterns of stainless steel, (a) cold rolled (CR) deformation of 78%, (b) cold rolled deformation of 78% and solution treatment (ST)

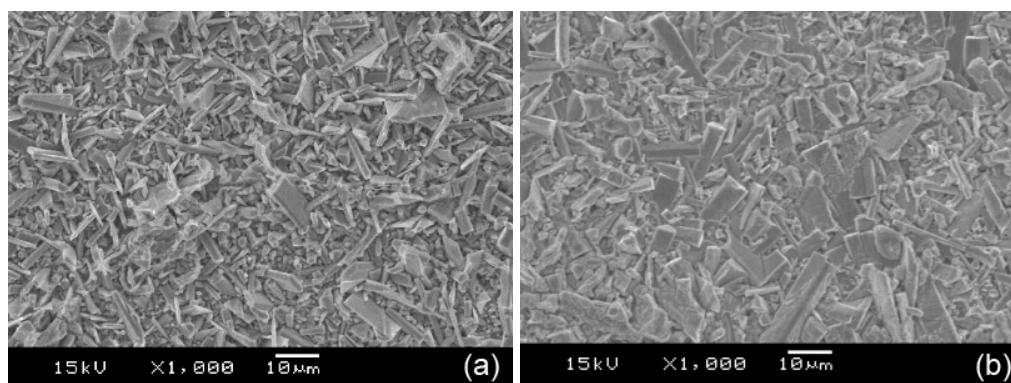


Figure 6. The surface morphology of the compound on different stainless steels, (a) cold rolled deformation of 78%, (b) cold rolled deformation of 78% and solution treatment.

3.3 Electrochemical corrosion property

The polarization curves of 304 stainless steels with 0%, 36%, 55%, and 78% deformation in 3.5% NaCl solution are shown in Fig. 7. The characteristic parameters as self-corrosion potential and pitting potential can be observed from the polarization curves. Self-corrosion potential has small difference for the cold rolled stainless steel, but the pitting potential is quite different. The stainless steel with 0% cold rolled deformation has the highest pitting potential. At low deformations (36% and 55% CR), the pitting potential is decreased compared with the stainless steel without cold rolling. The cold rolling reduces the corrosion resistance of stainless steel. At the cold rolling of 78% in this study,

it has the similar pitting potential with no deformation stainless steel.

Pitting potential and Fe-Sn intermetallics (IMC) thickness as a function of cold rolling reduction is shown in Fig. 8. Comparing the relationship curves, the cold rolled stainless steel has the highest pitting potential and the thickness of the growth compound is the lowest. As the cold rolling deformation increases, the pitting potential gradually increases, and the compound thickness gradually decreases.

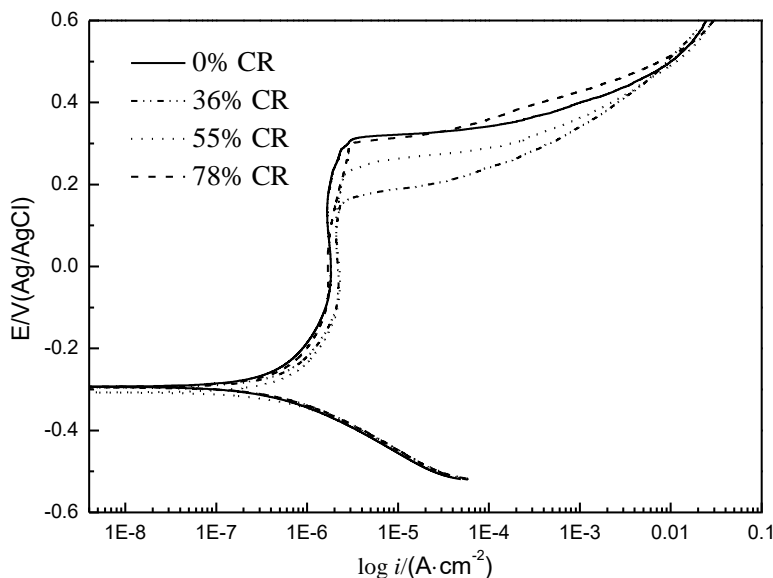


Figure 7. Potentiodynamic polarization curves of 304 stainless steel with cold rolled deformation

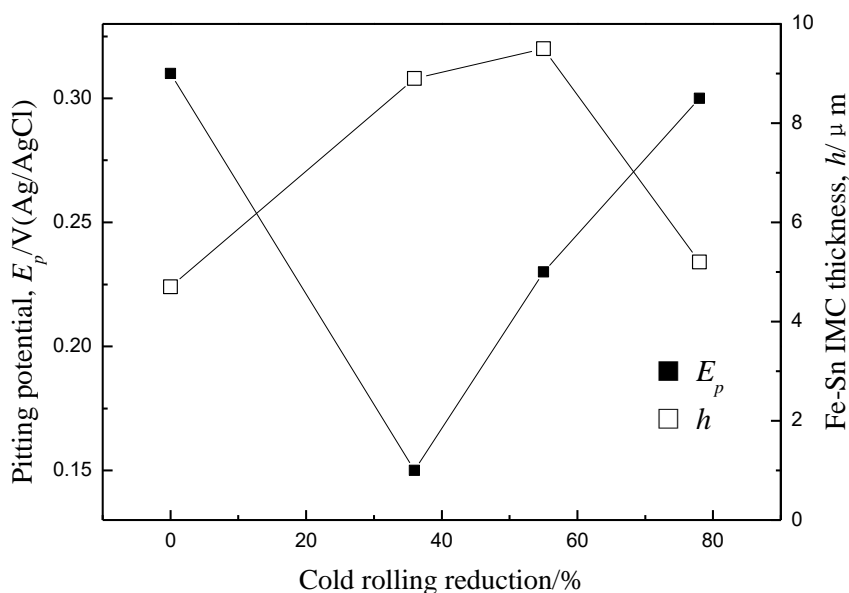


Figure 8. Pitting potential E_p and Fe-Sn IMC thickness h as a function of cold rolling reduction

The growth the interfacial Fe-Sn compound can be influenced by two procedures: one is the atomic diffusion and the other is the atomic reaction. The growth of Fe-Sn compound layer was controlled by atomic diffusion, because a linear relationship between the intermetallics thickness and

the reaction time was proved in the preliminary work [19]. Chen et al. [20] also proposed that the diffusion dominated the interfacial compound layer growth. Through the diffusion path, the reaction at the interface for Fe atoms and Sn atoms to form Fe-Sn intermetallics. When the stainless steel is cold rolled deformation, the defects and vacancies in the stainless steel are reduced, which reduces the diffusion channel between Sn atom and Fe atom, resulting in a decrease in the thickness of the compound. The effect of texture becomes prominent at higher deformations [21]. Ogunsanya and Hansson [22] proposed that the crystallographic texture enhances Cr diffusion in Fe-Cr alloys, which then influences the passivation behavior of 304 stainless steel. The passive films contained a higher Cr/Fe ratio are grown on high deformation stainless steel. The pitting potential increases on the stainless steel with the cold rolling deformation of 78%. The pitting potential of stainless steel is increased, and the corrosion resistance of stainless steel is increased.

4. CONCLUSION

(1) The cold rolling reduction of austenitic stainless steel leads to the development of the α' -martensitic transformation. The austenite γ -phase diffraction peaks decrease or disappear after cold rolled deformation. The solution treatment makes α' -martensite recrystallization.

(2) The interaction of liquid Sn with deformed stainless steel produces the formation of intermetallics (Fe, Cr)Sn₂ layer. The effect of α' -martensite is expected to cause significant changes in Fe-Sn intermetallics morphology.

(3) At low deformations of 36% and 55%, the cold rolling is found to decrease in pitting potential, and deteriorates electrochemical behavior of stainless steels. The Fe-Sn intermetallics thickness is increased compared with no deformation stainless steel. At the deformation of 78%, the pitting resistance is increased, and the compound thickness expresses a small change.

ACKNOWLEDGMENT

This work was supported by Liaoning Province Department of Education Research Funding Project (NO. L2019045), Science and Technology Research Fund of Liaoning Province Department of Education (NO. L2017LQN026) and Scientific Research Cultivation Fund of LSHU (No.2016PY-024).

References

1. A. Gruttadauria, S. Barella and R. Gerosa, *Eng. Fail. Anal.*, 100 (2019) 88.
2. S.H. Kim, G.O. Subramanian, C. Kim, C. Jang and K.M. Park, *Surf. Coating Tech.*, 349 (2018) 415.
3. S. Wang, H. Xue, Y.H. Cui, W. Tang and X.Y. Gong, *Procedia Struct. Integ.*, 12 (2018) 1940.
4. Y. Zhang, M. Li, H.Y. Bi, D.X. Chen, J.Q. Gu and E. Chang, *Mater. Sci. Eng. A*, 759 (2019) 224.
5. Q.C. Wang, B.C. Zhang, Y.B. Ren and K. Yang, *Corr. Sci.*, 145 (2018) 55.
6. L. Peguet, B. Malki and B. Baroux, *Corr. Sci.*, 49 (2007) 1933.
7. S.Y. Wang, Y.J. Hu, K.W. Fang, W.Q. Zhang and X.L. Wang, *Corr. Sci.*, 126 (2017) 104.
8. M. Maric, O. Muransky and I. Karatchevtseva, *Corr. Sci.*, 142 (2018) 133.
9. G. Monrrabal, A. Bautista, S. Guzman, C. Gutierrez and F. Velasco, *Mater. Res. Tech.*, 8 (2019)

1335.

10. D.G. Rodrigues, G.G.B. Maria, N.A.L. Viana and D.B. Santos, *Mater. Charact.*, 150 (2019) 138.
11. G. Du, J. Li, W.K. Wang, C. Jiang and S.Z. Song, *Corro. Sci.*, 53 (2011) 2918.
12. A. Turnbull, M. Ryan, A. Willetts and S. Zhou, *Corro. Sci.*, 45 (2003) 1051.
13. X.G. Feng, X.Y. Zhang, Y.W. Xu, R.L. Shi, X.Y. Lu, L.Y. Zhang, J. Zhang and D. Chen, *Eng. Fail. Anal.*, 98 (2019) 49.
14. J. Luo, H. Cheng, K.M. Asl, Y.C.J. Kiel and M.P. Harmer, *Science*, 1730 (2011) 333.
15. M. Hida and M. Kajihara, *Mater. Trans.*, 53 (2012) 1240.
16. T. Auger, Z. Hamouche, A. Medin and D. Gorse, *J. Nucl. Mater.*, 253 (2008) 377.
17. Y. Zhao, J.J. Guan, F. Liu, C.Q. Cheng and J. Zhao, *High Temp. Mater. Process.*, 37 (2018) 1.
18. Y. Zhao, D.Y. Zhang, J.J. Guan, F. Liu, P. Liang, C.Q. Cheng and J. Zhao, *Int. J. Electrochem. Sci.*, 14 (2019) 301.
19. J.J. Guan, Y. Zhao, F. Liu and J. Zhao, *Met. Mater. Int.*, 21 (2015) 1006.
20. L.D. Chen, M.L. Huang and S.M. Zhou, *J. Alloy Compd.*, 501 (2010) 535.
21. B. Ravikumar, B. Mahato and R. Singh, *Mettal. Mater. Trans. A*, 38 (2007) 2085.
22. I.G. Ogunsanya and C.M. Hansson, *Materialia*, 6 (2019) 100321.

© 2019 The Authors. Published by ESG (www.electrochemsci.org). This article is an open access article distributed under the terms and conditions of the Creative Commons Attribution license (<http://creativecommons.org/licenses/by/4.0/>).